Optica Applicata, Vol. XLV, No. 3, 2015
DOI: 10.5277/oa150302

Hybrid heptafocal intraocular lenses

MACIEJ SOKOŁOWSKI*, JACEK PNIEWSKI, RAFAŁ BRYGOŁA,
MAREK KOWALCZYK-HERNÁNDEZ

Faculty of Physics, University of Warsaw, Pasteura 7, 02-093 Warszawa, Poland

*Corresponding author: msokol@igf.fuw.edu.pl

In this paper, hybrid diffractive-refractive multifocal intraocular lenses are proposed, which are intended to provide good visual acuity over a discrete spectrum of object distances most often encountered by patients. The proposed hybrid lenses have seven foci. It is shown that by the appropriate selection of modulation depth of a sinusoidal phase diffractive profile and the period of the sinusoid, sharp vision can be achieved for a set of distances such as 24, 29, 37, 49, 73, 145 cm, and infinity. Theoretical axial and lateral visual point spread functions are computed. An accommodative amplitude equivalent of the eye implanted with a multifocal intraocular lens is introduced and calculated for the proposed heptafocal intraocular lenses.

Keywords: diffractive lens, hybrid lens, multifocal intraocular lens.

1. Introduction

Implantation of an artificial intraocular lens (IOL) during the eye surgery should, in principle, reconstruct all the functions of the natural crystalline lens, including accommodation [1]. Nevertheless to provide a sharp vision over the full range of object distances still remains a challenge for microoptics and cataract surgery. Several models of bifocal and trifocal IOLs were proposed, namely refractive IOLs [2, 3], hybrid refractive-diffractive IOLs [4,5], and apodized refractive-diffractive IOLs [4–7]. In bifocal refractive-diffractive lenses, the power of the refractive component provides a sharp distant vision, and the power of the diffractive component is equal to the addition needed for near vision. In apodized lenses, the diffraction efficiency changes with the radius of the lens in such a way that for dim light conditions, when the diameter of the pupil is large, more light is directed to the focus for the far vision. There also are diffractive IOLs implanted into the anterior chamber [8] or fixed in the ciliary sulcus in the posterior chamber [9, 10] and diffractive intracorneal lenses (ICLs) [11]. If the ciliary muscle is working correctly, accommodating lenses can be implanted, *e.g.*, Crystalens where the power or position of the lens is changed mechanically [12]. The most technologically advanced commercial hybrid lenses are apodized trifocals, which assure sharp vision for far distance, near distance and for a certain intermediate distance (*e.g.*, FineVision (Micro F) by PhysIOL) [6]. There exists a separate class of

hybrid lenses – candidates for IOLs. Those are the IOLs which provide additional power by means of either refractive or diffractive axicon-based lens that extends substantially the focal depth without modification of numerical aperture [13, 14].

In this paper we present novel hybrid multifocal IOLs, which are intended to provide good visual acuity at a discrete spectrum of distances most often encountered by patients. It is shown that by the appropriate selection of modulation depth of a sinusoidal phase diffractive profile, sharp vision can be achieved at distances: 24 cm (reading texts written with small fonts), 29 and 37 cm (reading distance), 49 and 73 cm (computer screen distance), 145 cm (intermediate distance) and far distance. We derive formulae for a visual point spread function of the IOLs of the arbitrary number of foci that include the parameters of both refractive and diffractive components of a hybrid lens, thus our approach may be considered a generalization of that presented in [15] for the trifocal IOLs.

2. Concept of a hybrid multifocal intraocular lens

Diffractive components of commercially available hybrid IOLs are axially symmetric analogs of blazed diffraction gratings. Hence, they diffract virtually all the energy of an incident parallel beam towards nonnegative diffraction orders only (Figs. 1**a** and 1**b**). The depth of the diffraction surface relief is usually optimized in such a way as to assure the necessary balance between the light energy diffracted to the 0th and to the 1st diffraction order. A consequence of this standard design is that a trifocal lens must be a superposition of two diffraction lenses with different carriers [6].

The idea to use a diffractive IOL with a sinusoidal diffraction relief shaped as full sinusoidal oscillations of one carrier, and not as descending half-periods (see Fig. 1**b** [16]), can be found in papers [15] and [17]. In those papers, three foci appear as –1st, 0th, and +1st diffraction orders (Fig. 1**c**). Higher orders were to be neglected

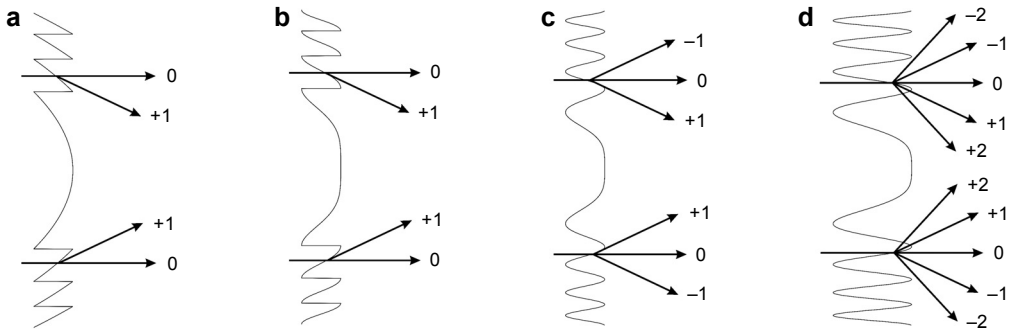

Fig. 1. Schematic representation of diffraction of a parallel light beam by intraocular diffractive lenses with basic surface profiles; Fresnel parabolic lens (**a**); cosine-step phase plate (**b**); sinusoidal phase plate of moderate phase modulation depth (~π rad) (**c**); sinusoidal phase plate of large modulation depth ($\geq 2\pi$ rad) proposed in this paper (**d**). The numbers 0, ±1, and ±2 indicate the diffraction orders.

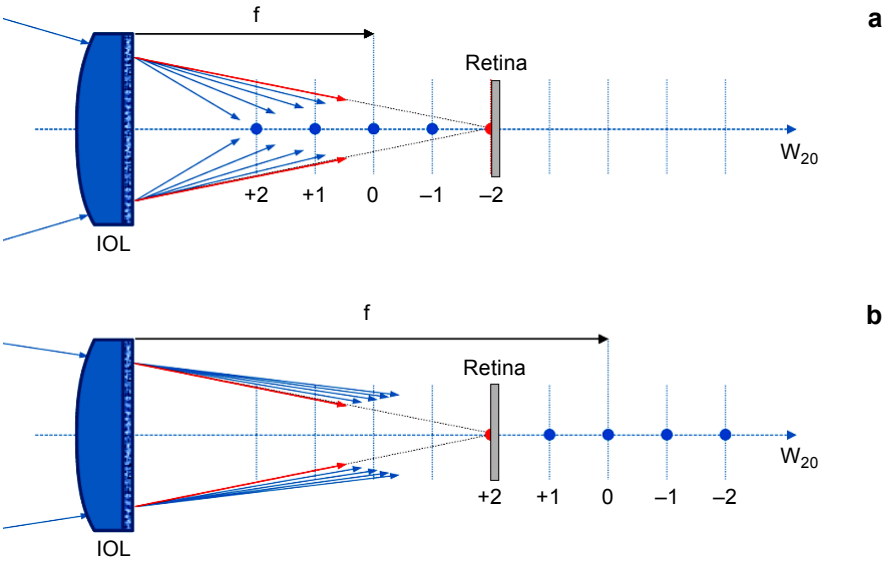

Fig. 2. Rays from an axial point object converged by the cornea and the refractive component of the hybrid IOL are diffracted into five coaxial beams of different vergences. The numbers 0, ±1, ±2 indicate the foci where the beams of corresponding diffraction orders are focused, f is the distance from the lens to the zeroth order focus for a given distance of the object from the eye. Optical axis is scaled in the optical defocus units W_{20}, thus the foci are equidistant [18]; object at infinity (**a**), and object at the nearest point sharply imaged on the retina (**b**).

as the phase modulation depth was relatively small. In our model we propose the use of a high modulation depth for which the phase modulation becomes a strongly non-linear process so that diffraction orders higher than ±1st appear (Fig. 1**d**). Negative order beams are focused in real foci in the image space, provided that the diffractive lens is illuminated by a sufficiently convergent beam (see Fig. 2). This is the case in standard ocular conditions.

The operation concept of a hybrid multifocal lens is shown in Fig. 2 for a lens with five foci. An incident object beam with the highest vergence (far object) after passing the lens is diffracted in such a way that the diffraction focus of –2nd order coincides with the plane of the retina. When the object moves closer to the eye (intermediate and near distances), the vergence of the object beam in the plane of the anterior surface of the cornea becomes more negative and the foci move away from the lens. Thus, the subsequent focused beams diffracted to the –1st, 0th, +1st, and +2nd diffraction order appear in the plane of the retina.

The above description is an ideal model. The challenge is to find such a modulation depth for which all the orders of interest are of virtually the same diffraction efficiency. In the section to follow we show how diffraction efficiency of high diffraction orders can be controlled by a proper choice of the phase modulation depth.

3. Axial point spread function calculation

We shall use the theoretical approach developed in [18]. Let ξ, η denote Cartesian coordinates in the plane of the lens, x, y denote Cartesian coordinates in the observation plane, and z' denotes the distance from the lens to the observation plane. We assume that in the case of monochromatic illumination of the wavelength λ, the complex amplitude of the light wave $U(x, y, z')$ in the image space is related to the amplitude $U'(\xi, \eta; z' = 0)$ immediately after the thin hybrid lens by the Fresnel approximation integral [19]:

$$U(x, y, z') = \frac{\exp(ikz')}{i\lambda z'} \exp\left[\frac{ik}{2z'}(x^2 + y^2)\right] \times \times \iint U'(\xi, \eta) \exp\left[\frac{ik}{2z'}(\xi^2 + \eta^2)\right] \exp\left[-\frac{2\pi i}{\lambda z'}(x\xi + y\eta)\right] \mathrm{d}\xi \mathrm{d}\eta \tag{1}$$

where $k = 2\pi/\lambda$. Neglecting the complex factor in front of the integral and assuming that amplitude transmittance of the diffractive lens is a function of the radial coordinate only, one can obtain

$$U(x, y, z') = \frac{1}{\lambda z'} \iint U'(\sqrt{\xi^2 + \eta^2}) \exp\left[\frac{ik}{2z'}(\xi^2 + \eta^2)\right] \times \times \exp\left[-\frac{2\pi i}{\lambda z'}(x\xi + y\eta)\right] \mathrm{d}\xi \mathrm{d}\eta \tag{2}$$

The integral in Eq. (2) is the Fourier transform of the product of rotationally symmetric functions, thus it can be rewritten as the Fourier–Bessel (FB) transform of this product, for the radial spatial frequency $\rho_r = \rho/\lambda z'$, where ρ is the radial polar coordinate in the observation xy plane [19]. With the radial polar coordinate r in the $\xi\eta$ plane we obtain

$$U(\rho, z') = \frac{1}{\lambda z'} \mathrm{FB}\left[U'(r) \exp\left(\frac{ik}{2z'} r^2\right)\right]\Bigg|_{\rho_r = \rho/\lambda z'} = = \frac{2\pi}{\lambda(f + z)} \int_0^\infty U'(r) \exp\left[\frac{ik}{2(f + z)} r^2\right] J_0\left(2\pi \frac{\rho}{\lambda(f + z)} r\right) r \, \mathrm{d}r \tag{3}$$

where J_0 is a Bessel function of the first kind, zeroth order. In the right-hand side of Eq. (3), z' is replaced by $(f + z)$, where f is the distance from the lens to the paraxial image of an axial point object formed by the refractive lens, which means that now axial distances z are measured with respect to the Gaussian image plane of the refractive lens. The distance f depends on the vergence of an incident beam and on the power of the refractive component of the hybrid lens. The smaller the vergence the larger is f

(see Fig. 2). For an axial point object, the field amplitude immediately after the hybrid lens is as follows:

$$U'(r) = \frac{\mathrm{circ}(r/R)}{f}\exp\left(\frac{-ik}{2f}r^2\right)\exp[i\phi(r)] =$$

$$= \frac{\mathrm{circ}(r/R)}{f}\exp\left(\frac{-ik}{2f}r^2\right)\exp\left\{\frac{im}{2}\cos\left[2\pi n\left(\frac{r}{R}\right)^2\right]\right\} \tag{4}$$

where the right-hand side exponent function is the amplitude transmittance of the sinusoidal phase diffractive lens of the radius R and the number of zones n. The diffractive lens introduces the phase delay $\phi(r)$ of the incident beam with peak-to-peak modulation depth m (Fig. 3).

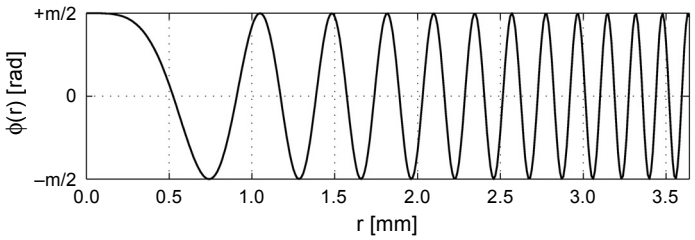

Fig. 3. Phase delay $\phi(r)$ introduced by the 12-zone diffractive lens of the radius 3.63 mm.

Let us substitute $q = (r/R)^2$ and use the Fresnel number $N = R^2/\lambda f$. With these substitutions Eqs. (3), (4), and (5) yield the 3-D amplitude impulse response of the hybrid lens

$$U(\rho, z; f, n, m) = \frac{\pi N}{f+z} \times$$

$$\times \int_0^1 \exp\left[\frac{im}{2}\cos(2n\pi q)\right]\exp\left[-i\pi N\left(\frac{z}{f+z}\right)q\right]J_0\left(2\pi\frac{R\rho}{\lambda(f+z)}\sqrt{q}\right)\mathrm{d}q \tag{5}$$

Equation (5) is our basic formula which we use as a starting point to calculate both axial point spread function $\mathrm{PSF_a}$ and lateral point spread function $\mathrm{PSF_l}$ (for z at which the diffraction foci are centered) and to choose a proper modulation depth $m/2$. The 3-D PSF, I, is equal to

$$I(\rho, z; f, n, m, N) = |U(\rho, z; f, n, m, N)|^2 =$$

$$= \left(\frac{\pi N}{f+z}\right)^2\left|\int_0^1 \exp\left[\frac{im}{2}\cos(2n\pi q)\right]\exp\left[-i\pi N\left(\frac{z}{f+z}\right)q\right]J_0\left(2\pi\frac{R\rho}{\lambda(f+z)}\sqrt{q}\right)\mathrm{d}q\right|^2 \tag{6}$$

We obtain the $\mathrm{PSF_a}$ by letting $\rho = 0$ in Eq. (6). As the $J_0(0) = 1$ we have

$$\mathrm{PSF_a}(z;\, f,\, n,\, m,\, N) \;=\; \left| \frac{\pi N}{f+z} \int_0^1 \exp\left[\frac{im}{2} \cos(2n\pi q) \right] \exp\left[-i\pi N \left(\frac{z}{f+z} \right) q \right] \mathrm{d}q \right|^2 \tag{7}$$

Equation (7) is a convenient formula to calculate numerically the $\mathrm{PSF_a}$ *versus* z. Nevertheless we need an analytic formula useful for a proper choice of phase modulation depth $m/2$. To reach this purpose, we notice that the Fourier transform kernel in Eq. (7) can be expressed in terms of the defocus coefficient W_{20}, being also the coefficient of R^2 term in the Taylor expansion of the wave aberration of a rotationally symmetric system [20]:

$$W_{20} \;=\; \frac{1}{2} \left(\frac{z}{f+z} \right) N \tag{8}$$

We shall use hereafter W_{20} as a new measure of the axial distance from the 0th order focus. Only for $|z| \ll f$, hence at the close vicinity of the origin, the mapping $z \to W_{20}$ is linear. With the use of W_{20} in Eq. (7) we obtain

$$\begin{aligned} &\mathrm{PSF_a}(W_{20};\, f,\, n,\, m,\, N) \;= \\ &= \left| \frac{\pi(N - 2W_{20})}{f} \int_0^1 \exp\left[\frac{im}{2} \cos(2n\pi q) \right] \exp[-2\pi i W_{20} q]\, \mathrm{d}q \right|^2 \;= \\ &= \left| \frac{\pi(N - 2W_{20})}{f} \left[\exp(-\pi i W_{20}) \operatorname{sinc}(W_{20}) \right] \otimes \Im \left\{ \exp\left[\frac{im}{2} \cos(2n\pi q) \right] \right\} \right|^2 \end{aligned} \tag{9}$$

where $\Im$ is the Fourier transform operator and $\otimes$ stands for the convolution. It is seen that for large Fresnel numbers, such that $2|W_{20}| \ll N$, the $\mathrm{PSF_a}$ is the squared modulus of 1-D Fourier transform (in the W_{20} space) of the properly mapped pupil function of a diffraction limited system. The Fourier transform in the right-hand side of the above convolution can be computed by means of the Jacobi–Anger expansion

$$\exp[i\beta \cos(\theta)] \;=\; \sum_{s=-\infty}^{\infty} i^s J_s(\beta) \exp(is\theta) \tag{10}$$

as follows:

$$\begin{aligned} \mathrm{PSF_a}(W_{20};\, f,\, n,\, m,\, N) \;&=\; \left[\frac{\pi(N - 2W_{20})}{f} \right]^2 \times \\ &\times \left| \exp(-\pi i W_{20}) \operatorname{sinc}(W_{20}) \otimes \Im \left\{ \sum_{s=-\infty}^{\infty} i^s J_s\left(\frac{m}{2} \right) \exp[2\pi i s (nq)] \right\} \right|^2 \;= \end{aligned}$$

$$= \left| \frac{\pi(N-2W_{20})}{f} \left\{ \sum_{s=-\infty}^{\infty} i^s \exp[-\pi i(W_{20}-sn)] J_s\left(\frac{m}{2}\right) \operatorname{sinc}(W_{20}-sn) \right\} \right|^2 \approx$$

$$\approx \left[\frac{\pi(N-2W_{20})}{f} \right]^2 \sum_{s=-\infty}^{\infty} J_s^2\left(\frac{m}{2}\right) \operatorname{sinc}^2(W_{20}-sn) \tag{11}$$

The final approximation in Eq. (11) holds when the number of zones n is sufficiently large and consequently the diffraction orders are well separated from each other along the optical axis. This is the case for the number of zones $n \geq 4$. It is seen that the diffraction efficiency of the $\pm s$ diffraction orders equals $J_s^2(m/2)$. This result is formally the same as that for the thin sinusoidal phase grating [19]. The only difference is the factor $(N-2W_{20})^2$ which causes that positive diffraction orders, located on the negative W_{20} semiaxis, are stronger than the corresponding negative orders located on the positive semiaxis.

In Figure 4 the curves $J_s^2(m/2)$ are presented for $s = 0, \pm1, \pm2, \pm3$, and ±4. It is seen that there is no $m/2$ for which $J_0^2(m/2) \approx J_{\pm1}^2(m/2) \approx J_{\pm2}^2(m/2) \approx J_{\pm3}^2(m/2)$, thus it is not possible to produce a diffractive lens with seven foci of the same diffraction efficiency. Nevertheless we can find $m/2$ such that $J_0^2(m/2) \approx J_{\pm1}^2(m/2) \approx 0.4J_{\pm2}^2(m/2) \approx \approx J_{\pm3}^2(m/2)$. This is the case for $m/2 = 3.1128$ rad (the second root of the equation $J_0^2(m/2) = J_1^2(m/2)$). Thus one can obtain a diffractive lens with seven foci such that foci of ±2nd orders are dominant (see Fig. 5**a**). For $m/2 = 3.1128$ rad we have that $(J_0^2 + 2J_1^2 + 2J_2^2 + 2J_3^2) \times 3.1128 = 0.95$, thus 95% of the energy of the beam that passes through the IOL is diffracted towards the seven foci of interest.

Another modulation depth of interest is $m/2 = 3.8317$ rad (the second root of the equation $J_1^2(m/2) = 0$) for which $J_0^2(m/2) \approx J_{\pm2}^2(m/2) \approx J_{\pm3}^2(m/2) \approx 2.5J_{\pm4}^2(m/2)$.

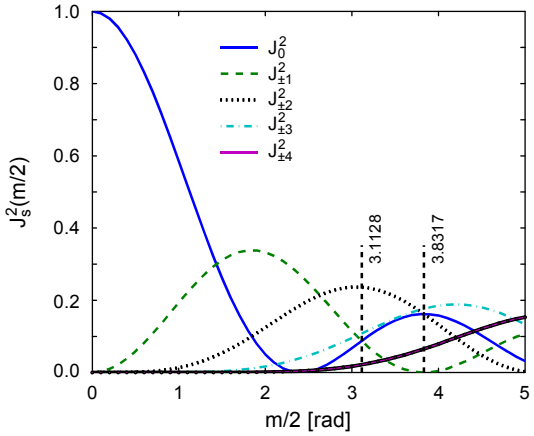

Fig. 4. Diffraction efficiency of the diffraction orders $s = 0, \pm1, \pm2, \pm3$, and ±4 as a function of modulation depth $m/2$ (Eq. (11)). Values $m/2$ equal to 3.1128 and 3.8317 rad are the modulation depths chosen for two models of heptafocal IOLs.

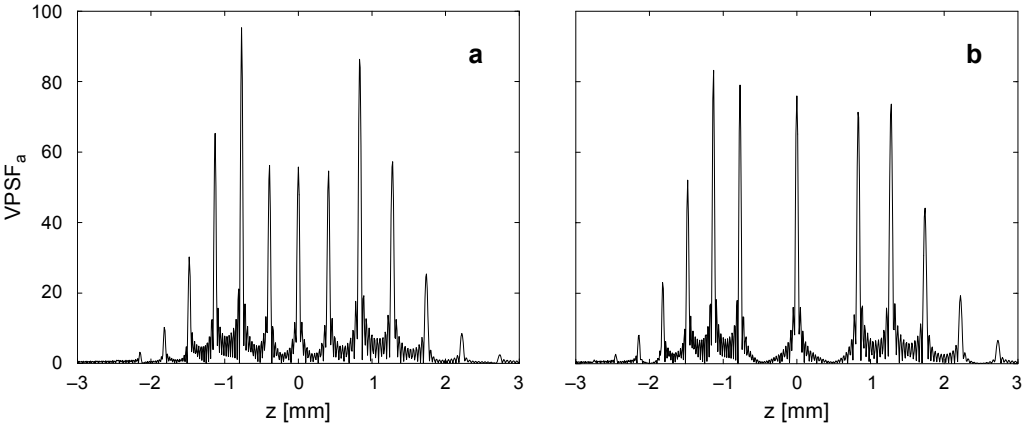

Fig. 5. Theoretical $VPSF_a$ for an axial point object, computed *versus* the real distance z, for hybrid heptafocal IOLs; $m/2 = 3.1128$ rad (**a**), and $m/2 = 3.8317$ rad (**b**).

Thus one can obtain a diffractive lens with seven foci such that foci of ±4th orders are of 2.5 times smaller diffraction efficiency than the foci of orders 0, ±2, and ±3 (see Fig. 5**b**). For $m/2 = 3.8317$ rad $(J_0^2 + 2J_2^2 + 2J_3^2 + 2J_4^2) \times 3.8317 = 0.97$, thus 97% of the energy of the beam that passes through the IOL is diffracted towards the seven foci of interest.

For a typical refractive index of lens material equal to 1.46 and that of vitreous equal to 1.336, topographical height of surface relief of the lens equal to 5.41 μm results in the required phase modulation depth equal to 3.8317 rad.

It is well-known that the sensation of brightness is not proportional to the intensity of incident light. Thus a visual PSF (VPSF) that takes into account an adequate relation between sensation of brightness and intensity of light will be a proper one to characterize an IOL from the quality of the retinal image point of view. Assuming the Stevens' power low relation between the physical stimulus and the psychophysical sensation and assuming the Stevens' exponent equal to 0.5 [21], we shall compute both axial and lateral VPSFs equal to the square root of the corresponding PSFs.

4. Lateral point spread function calculation

We shall calculate the lateral cross-sections of the 3-D PSF at those W_{20} where the foci are centered, *i.e.* at $W_{20} = tn$ ($t = 0, \pm1, \pm2, \pm3, \pm4$). Using Eq. (8), one can show that

$$\frac{R}{\lambda(z+f)} = \frac{N - 2W_{20}}{R} \tag{12}$$

Substitution of Eqs. (8) and (12) into Eq. (5) yields

$$U(\rho, W_{20}; f, n, m, N) = \frac{\pi(N-2W_{20})}{f} \times$$
$$\times \int_0^1 \exp\left[\frac{im}{2}\cos(2n\pi q)\right] \exp[-i2\pi W_{20} q] J_0\left[2\pi \frac{(N-2W_{20})\rho}{R}\sqrt{q}\right] \mathrm{d}q \tag{13}$$

For $W_{20} = tn$ we obtain the formula which is convenient for numerical calculation

$$\mathrm{PSF}_1(\rho, tn; f, n, m, N) = \left|U(\rho, W_{20} = tn; f, n, m, N)\right|^2 = \left[\frac{\pi(N-2tn)}{f}\right]^2 \times$$
$$\times \left| \int_0^1 \exp\left[\frac{im}{2}\cos(2n\pi q)\right] \exp[-i2\pi tnq] J_0\left[2\pi \frac{(N-2tn)\rho}{R}\sqrt{q}\right] \mathrm{d}q \right|^2 \tag{14}$$

In order to obtain a compact formal solution, we define a dimensionless radial coordinate

$$v \equiv 2\pi \frac{(N-2W_{20})}{R}\rho \tag{15}$$

which is a well-known radial optical coordinate expressed here in terms of W_{20}. For a given W_{20} the mapping $\rho \to v$ is linear. Substitution of the Jacobi–Anger expansion and Eq. (15) into Eq. (13) yields

$$U(v, W_{20}; f, n, m, N) = \left[\frac{\pi(N-2W_{20})}{f}\right] \times$$
$$\times \int_0^1 \sum_{s=-\infty}^{\infty} i^s J_s\left(\frac{m}{2}\right) \exp[2\pi i s(nq)] \exp[-i2\pi W_{20} q] J_0[v\sqrt{q}]\,\mathrm{d}q =$$
$$= \frac{2\pi(N-2W_{20})}{f} \sum_{s=-\infty}^{\infty} i^s J_s\left(\frac{m}{2}\right) \int_0^1 \exp[-i2\pi(W_{20}-sn)\zeta^2] \zeta J_0(v\zeta)\,\mathrm{d}\zeta =$$
$$= \frac{\pi(N-2W_{20})}{f} \sum_{s=-\infty}^{\infty} i^s J_s\left(\frac{m}{2}\right) [C(W_{20}-sn, v) - iS(W_{20}-sn, v)] \tag{16}$$

The real part $C(W_{20}, v)$ and the imaginary part $S(W_{20}, v)$ of the integral over ζ (Lommel diffraction integral), can be computed by means of the Lommel functions which in turn are defined as infinite series of Bessel functions of the first kind, integer

orders. For $N \gg 2|W_{20}|$ the result of Eq. (16) is a particular case of the axial sampling theorem as the field amplitude U at an arbitrary point (v, W_{20}) is calculated on the basis of the countable set of axial samples of U and interpolation function $[C(W_{20}, v) - iS(W_{20}, v)]$ centered at points $W_{20} = sn$ at which axial samples are taken [22]. For $W_{20} = tn$ we have:

$$\mathrm{PSF}_1(v, tn; f, n, m, N) =$$

$$= \left[\frac{\pi(N-2tn)}{f}\right]^2 \left| \sum_{s=-\infty}^{\infty} i^s J_s\left(\frac{m}{2}\right) [C(tn-sn, v) - iS(tn-sn, v)] \right|^2 \approx$$

$$\approx \left[\frac{\pi(N-2tn)}{f}\right]^2 \sum_{s=-\infty}^{\infty} J_s\left(\frac{m}{2}\right) |C(tn-sn, v) - iS(tn-sn, v)|^2 \tag{17}$$

This formal solution for the PSF_1 will be discussed in the last chapter of the paper.

5. Numerical simulation results

In order to calculate the VPSFs of heptafocal hybrid IOLs, we assume the following values of magnitudes of interest (in air): the wavelength $\lambda = 550$ nm, the number of zones $n = 12$, the first order power of diffractive lens equal to +1.0 dioptre (thus, the radius of the diffractive lens R is equal to $(12 \times 1.1)^{1/2}$ mm = 3.63 mm), the vergence of the light beam after passing the refractive component of the hybrid lens is equal to +50 dioptres, thus $f = 20$ mm and $N = 1200$. The above round values closely approximate the ocular ones and are chosen to demonstrate a diffractional behaviour of the proposed IOLs. Exact values of the Gullstrand–Emsley schematic eye are used in Chapter 6 in which we calculate the distances of sharp vision given by the multifocal IOL. The VPSF_a obtained for the above values and for $m/2 = 3.1128$ rad, calculated on the basis of Eq. (7), is shown in Fig. 5**a**. The ±2nd order foci are dominant as it was expected on the basis of Eq. (11). For $m/2 = 3.8317$ rad, the VPSF_a is shown in Fig. 5**b**. It is seen that the energy of diffracted light is uniformly divided among strong foci of orders 0, ±2, ±3 whereas a smaller amount of energy passes through the foci of ±4th orders (amounts of diffraction efficiency are presented in Table 1).

Functions VPSF_1 were computed on the basis of Eq. (14). For $m/2 = 3.1128$ and $t = 0, \pm1, \pm2$, and ±3 they are shown in Fig. 6 in which a reference Airy pattern is also

T a b l e 1. Diffraction efficiency of the diffraction orders $s = 0, \pm1, \pm2, \pm3$, and ± 4.

	Diffraction efficiency J_s^2					Amount of light
$m/2$	$s = 0$	$s = \pm1$	$s = \pm2$	$s = \pm3$	$s = \pm4$	in useful foci
3.1128	0.086	0.088	0.236	0.108	0.022	95%
3.8317	0.162	0.000	0.162	0.177	0.065	97%

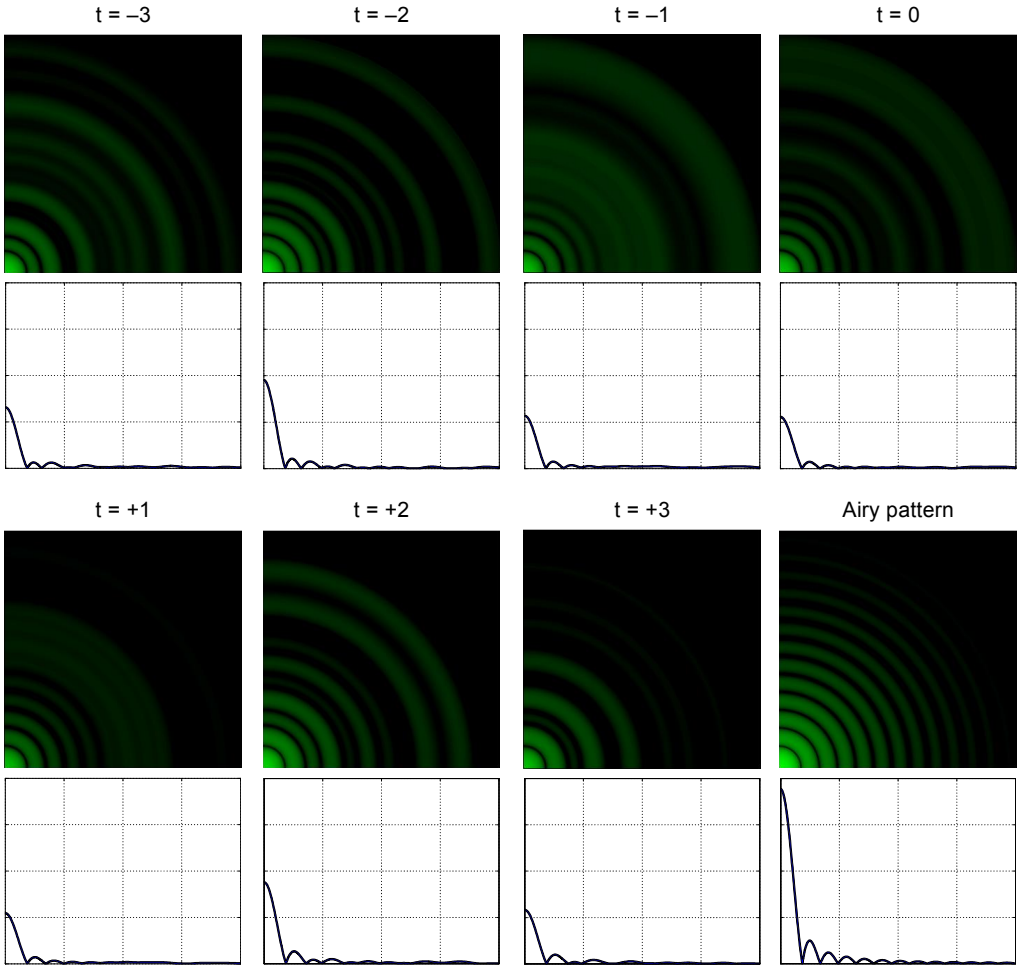

Fig. 6. Theoretical $VPSF_1$ for $m/2 = 3.1128$ at $W_{20} = nt$ ($t = 0, \pm1, \pm2$, and ±3). Due to a limited range of the color scale, the images show $\log(VPSF_1)$. Reference Airy diffraction pattern is computed by means of Eq. (14) for $m/2 = 0$ and $t = 0$. First zero of the Airy pattern is at $\rho = 1.85\times10^{-3}$ mm.

shown. Functions $VPSF_1$ for $m/2 = 3.8317$ and $t = 0, \pm2, \pm3$, and ±4 are very much alike to those of Fig. 6, except for $t = \pm1$, *i.e.* for $W_{20} = \pm1n$ for which there are only halo rings, *i.e.* the Airy-like maxima are absent.

6. Accommodative amplitude equivalent of the eye implanted with multifocal IOL

Heptafocal IOL successfully implanted into an eye with a spherical cornea should provide sharp vision at seven distances. The shortest and the longest distances may be considered analogs of the near point and far point distances of a phakic eye. Therefore,

an eye implanted with a multifocal IOL could be characterized by an amplitude A defined as the difference between the vergences of the farthest and the nearest point objects sharply imaged on the retina. This amplitude is equivalent to the amplitude of accommodation of a phakic eye and hereafter we shall call it an accommodative amplitude equivalent (AAE). We shall calculate the AAE of eyes implanted with proposed heptafocal IOLs using the Gullstrand–Emsley schematic eye. In that model, the cornea is a single refracting surface and the lens is thick and homogeneous. We assume that this lens is replaced by a thin hybrid IOL fixed at the distance 5.75 mm from the corneal vertex. The IOL separates the aqueous humour of refractive index 4/3 from the vitreous humour of refractive index 1.336.

First we calculate the AAE for a hybrid IOL with a diffractive lens having the modulation depth $m/2 = 3.1128$ rad and a refractive lens having power +23.75 dioptres (calculated according to the procedure described in [15]). For the above values, the method of back propagation of vergence yields the following set of sharp vision distances from the corneal vertex: –∞, –1.45, –0.73, –0.49, –0.37, –0.29, and –0.24 m. The minus signs result from the sign convention used in visual optics. Thus, neglecting the small distance of the first principal plane of the eye from the corneal vertex, we have that the AAE of the implanted eye is equal $A = (1/-\infty) - (1/-0.24) = 4.17$ D. Then, we repeat the calculation for a hybrid IOL consisting of a diffractive lens with the modulation depth $m/2 = 3.8317$ rad and a refractive lens with power +24.75 dioptres. In this case, the back propagation of vergence yields the following set of sharp vision distances: –∞, –1.45, –0.73, –0.37, –0.24, –0.21, and –0.18 m. Thus, $A = (1/-\infty) - (1/-0.18) = 5.56$ D.

7. Discussion and conclusions

Two models of hybrid heptafocal IOLs are proposed. In each model five of seven foci are of virtually the same diffraction efficiency and more than 95% of energy of transmitted light is diffracted towards the seven foci of interest. Computed functions VPSF_a (Fig. 5) and VPSF_1 (Fig. 6) and their approximations by infinite series (Eqs. (11) and (17)) show that all the foci are well defined and resemble those of single focus vision. Axial distribution of energy in each focal region is given by the squared sinus function and lateral distribution is that of Airy pattern surrounded by weak halos that are noticeable when the VPSF_1 is presented on a logarithmic scale. Therefore good imaging properties of heptafocal hybrid IOLs may be expected.

In our calculations, the Fresnel approximation is used which is commonly used in the analysis of the quality of an image formed on the retina of the eye, in particular of an eye in which the natural lens is replaced with an artificial implant. The Fresnel approximation is a small angle approximation of the wave optics. Consequently, we used the Gullstrand–Emsley schematic eye which was elaborated within a small angle approximation. For such approximation, various refractive surfaces used to model re-

fractive surfaces of the eye are virtually equivalent. The calculations lead to the conclusion that proposed heptafocal intraocular lenses could eliminate the dependence on spectacles after cataract surgery.

It seems that the increase in the number of foci by means of further increase of $m/2$ is possible but is not recommended as it may lead to the decrease in the signal-to-noise ratio. The reason is that each focus will receive smaller fraction of the energy transmitted through the lens, whereas the energy of a noisy halo will be approximately constant. On the other hand, further increase in the number of foci does not seem to be necessary from the point of view of the patient's needs as he or she can probably easily adjust the distance of the observed object to the one of the seven distances of sharp vision. Moreover, the focus of most negative order, which in principle is used for observation of very distant objects, in fact provides relatively sharp vision at any distance larger than approximately 4 m due to the depth of field of the human eye, which is equal to ±0.25 dioptres for typical diameter of the pupil. All the discussions and conclusions on achromatization and compensation for monochromatic corneal aberrations presented in the papers on bifocal and trifocal hybrid IOLs are also valid in the case of heptafocal hybrid IOLs. Diffractive heptafocal lenses described in this paper can be also implemented in contact lenses for presbyopic patients and perhaps in multifocal keratoprostheses [23].

The carried out calculations did not take into account the influence of other optical and physiological factors such as chromatic aberration, the size of the pupil or the halo effect. Therefore promising result presented here are preliminary.

References

[1] Apple D.J., Sims J., *Harold Ridley and the invention of the intraocular lens*, Survey of Ophthalmology **40**(4), 1996, pp. 279–292.

[2] Auffarth G.U., Dick H.B., *Multifokale intraokularlinsen: Eine Übersicht*, Der Ophthalmologe **98**(2), 2001, pp. 127–137.

[3] de Vries N.E., Nuijts R.M.M.A., *Multifocal intraocular lenses in cataract surgery: literature review of benefits and side effects*, Journal of Cataract and Refractive Surgery **39**(2), 2013, pp. 268–278.

[4] Davison J.A., Simpson M.J., *History and development of the apodized diffractive intraocular lens*, Journal of Cataract and Refractive Surgery **32**(5), 2006, pp. 849–858.

[5] Kohnen T., Allen D., Boureau C., Dublineau P., Hartmann C., Mehdorn E., Rozot P., Tassinari G., *European multicenter study of the AcrySof ReSTOR apodized diffractive intraocular lens*, Ophthalmology **113**(4), 2006, pp. 578–584.

[6] Gatinel D., Pagnoulle C., Houbrechts Y., Gobin L., *Design and qualification of a diffractive trifocal optical profile for intraocular lenses*, Journal of Cataract and Refractive Surgery **37**(11), 2011, pp. 2060–2067.

[7] Sheppard A.L., Shah S., Bhatt U., Bhogal G., Wolffsohn J.S., *Visual outcomes and subjective experience after bilateral implantation of a new diffractive trifocal intraocular lens*, Journal of Cataract and Refractive Surgery **39**(3), 2013, pp. 343–349.

[8] Morris G.M., Nordan L.T., *Phakic intraocular lenses: the new focus in refractive surgery*, Optics and Photonics News **15**(9), 2004, pp. 26–31.

[9] SCHRECKER J., KROEBER S., EPPIG T., LANGENBUCHER A., *Additional multifocal sulcus-based intraocular lens: alternative to multifocal intraocular lens in the capsular bag*, Journal of Cataract and Refractive Surgery **39**(4), 2013, pp. 548–555.
[10] GERTEN G., KERMANI O., SCHMIEDT K., FARVILI E., FOERSTER A., OBERHEIDE U., *Dual intraocular lens implantation: monofocal lens in the bag and additional diffractive multifocal lens in the sulcus*, Journal of Cataract and Refractive Surgery **35**(12), 2009, pp. 2136–2143.
[11] TANKAM P., LÉPINE T., CASTIGNOLES F., CHAVEL P., *Optical metrology for immersed diffractive multifocal ophthalmic intracorneal lenses*, Journal of the European Optical Society – Rapid Publications **7**, 2012, article 12037.
[12] MENAPACE R., FINDL O., KRIECHBAUM K., LEYDOLT-KOEPPL CH., *Accommodating intraocular lenses: a critical review of present and future concepts*, Graefe's Archive for Clinical and Experimental Ophthalmology **245**(4), 2007, pp. 473–489.
[13] FLORES A., WANG M.R., YANG J.J., *Achromatic hybrid refractive-diffractive lens with extended depth of focus*, Applied Optics **43**(30), 2004, pp. 5618–5630.
[14] GARCÍA J.A., BARÁ S., GÓMEZ GARCÍA M., JAROSZEWICZ Z., KOLODZIEJCZYK A., PETELCZYC K., *Imaging with extended focal depth by means of the refractive light sword optical element*, Optics Express **16**(22), 2008, pp. 18371–18378.
[15] VALLE P.J., OTI J.E., CANALES V.F., CAGIGAL M.P., *Visual axial PSF of diffractive trifocal lenses*, Optics Express **13**(7), 2005, pp. 2782–2792.
[16] CASTIGNOLES F., FLURY M., LEPINE T., *Comparison of the efficiency, MTF and chromatic properties of four diffractive bifocal intraocular lens designs*, Optics Express **18**(5), 2010, pp. 5245–5256.
[17] GOLUB M.A., GROSSINGER I., *Diffractive optical elements for biomedical applications*, Proceedings of SPIE **3199**, 1998, p. 220.
[18] MARTÍNEZ-CORRAL M., ANDRÉS P., OJEDA-CASTAÑEDA J., *On-axis diffractional behavior of two-dimensional pupils*, Applied Optics **33**(11), 1994, pp. 2223–2229.
[19] GOODMAN J.W., *Introduction to Fourier Optics*, McGraw-Hill, New York, 1996.
[20] ATCHISON D.A., SCOTT D.H., COX M.J., *Mathematical Treatment of Ocular Aberrations: A User's Guide*, OSA TOPS, Vol. 35, 2000, pp. 110–130.
[21] STEVENS S.S., *On the psychophysical law*, Psychological Review **64**(3), 1957, pp. 153–181.
[22] KOWALCZYK M., CICHOCKI T., MARTÍNEZ-CORRAL M., MUÑOZ-ESCRIVÁ L., *Sampling expansions for three-dimensional light amplitude distribution in the vicinity of an axial image point: comment*, Journal of the Optical Society of America A **20**(12), 2003, pp. 2390–2392.
[23] KOPANIA B., SOKOŁOWSKI M., PNIEWSKI J., AMBROZIAK A. M., IZDEBSKA J., KOWALCZYK-HERNÁNDEZ M., *Sztuczne implanty rogówkowe w praktyce klinicznej*, Kontaktologia i Optyka Okulistyczna, No. 4, 2013, pp. 15–22, (in Polish).

Received December 29, 2014
in revised form April 14, 2015